

Predicting Human Serum Albumin Affinity of Interleukin-8 (CXCL8) Inhibitors by 3D-QSPR Approach

Loretta Aureli,[†] Gabriele Cruciani,[‡] Maria Candida Cesta,[§] Roberto Anacardio,^{||} Lucio De Simone,^{||} and Alessio Moriconi^{*,§}

Molecular Discovery Ltd., 4, Chandos Street, W1A 3BQ, London, United Kingdom, Laboratory for Chemometrics and Cheminformatics, University of Perugia, Via Elce di Sotto, 10, I-06123 Perugia, Italy, and Chemistry Department and Analytical Department, Dompé Research and Development, Dompé S.p.A., via Campo di Pile, 67100, L'Aquila, Italy

Received September 22, 2004

A novel class of 2-(*R*)-phenylpropionamides has been recently reported to inhibit *in vitro* and *in vivo* interleukin-8 (CXCL8)-induced biological activities. These CXCL8 inhibitors are derivatives of phenylpropionic nonsteroidal antiinflammatory drugs (NSAIDs), high-affinity ligands for site II of human serum albumin (HSA). Up to date, only a limited number of *in silico* models for the prediction of albumin protein binding are available. A three-dimensional quantitative structure–property relationship (3D-QSPR) approach was used to model the experimental affinity constant (K_i) to plasma proteins of 37 structurally related molecules, using physicochemical and 3D-pharmacophoric descriptors. Molecular docking studies highlighted that training set molecules preferentially bind site II of HSA. The obtained model shows satisfactory statistical parameters both in fitting and predicting validation. External validation confirmed the statistical significance of the chemometric model, which is a powerful tool for the prediction of HSA binding in virtual libraries of structurally related compounds.

Introduction

HSA is the most abundant protein in human serum plasma.¹ HSA binds a wide range of endogenous and exogenous compounds.^{1,2} By virtue of its exceptional conformational adaptability, HSA strongly binds cations (Ca^{2+} , Na^+ , K^+), fatty acids, hormones, and many xenobiotics, including drugs. In addition to its unique binding capability, HSA has an interesting enzymatic “esterase-like” activity toward a large variety of substrates.³

Plasma protein binding is a significant factor in the transport and release of many drugs in the human body, strongly influencing their distribution and excretion and, by consequence, their pharmacological and toxicological profile. Since the pharmacological effect is attributed to the unbound drug fraction, plasma protein binding can affect the pharmacodynamics of many drugs.

HSA is constituted of a single polypeptidic chain (585 amino acids) with a molecular mass of 65 kDa.^{4,5} Its amino acids sequence includes a large number of charged amino acids: about 100 acidic residues (aspartates and glutamates) and about 100 basic residues (arginines, lysines and histidines). The 3D structure of HSA contains three homologous domains (I–III), each including two subdomains (A and B) with common structural motifs.^{4,5} The main drug binding regions are located in subdomains IIA (site I) and IIIA (site II); both binding sites are located in hydrophobic cavities able to accommodate a large range of chemical structures.^{4,5}

It has been shown that some drugs, such as warfarin,⁶ aspirin,⁷ and β -lactam antibiotics,^{5,8} prefer to bind to site I,⁹ while general anaesthetics¹⁰ and benzodiazepines¹¹ interact with site II. To date, however, limited and conflicting information about the exact binding mode of drugs with HSA sites has been reported in the literature.^{12–15}

Several widely used NSAIDs,¹⁶ such as ibuprofen and ketoprofen, belonging to the chemical class of 2-phenylpropionic acids, are highly bound to plasma proteins. The carboxylic moiety of NSAIDs is believed to play a key role in the binding to site II of HSA.¹⁶

Interleukin-8 (CXCL8) is a proinflammatory chemokine that is a major mediator of PMN recruitment in several acute and chronic inflammatory disorders. Several studies suggest a key role of CXCL8 in PMN recruitment and tissue injury occurring in postischemic reperfusion injury.¹⁷ In addition, CXCL8 induces keratinocyte proliferation as well as angiogenesis and has been strongly implicated in melanoma progression and metastasis.¹⁸ CXCL8 exerts its biological effects by activating two specific receptors, CXCR1 and CXCR2, belonging to the family of seven transmembrane G-protein-coupled receptors (7TM-GPCRs).¹⁹ CXCL8 is considered a primary target for a novel therapeutic approach for various human diseases.^{20,21} *N*-[(*R*)-2-(4-Isobutylphenyl)propionyl]methanesulfonamide (**2**), which belongs to a novel class of small molecular weight CXCL8 inhibitors, is currently undergoing clinical trials for the prevention of delayed graft function (DGF) occurring during organ transplant. **2** has recently been described as a potent noncompetitive allosteric inhibitor of CXCL8 acting in the trans-membrane region of CXCR1.²²

In this paper we show that several CXCL8 small molecular weight inhibitors, structurally related to

* Corresponding author. Phone: +39 0862 338424. Fax: +39 0862 338219. E-mail: alessio.moriconi@dompe.it.

[†] Molecular Discovery Ltd.

[‡] University of Perugia.

[§] Chemistry Department, Dompé Research and Development.

^{||} Analytical Department, Dompé Research and Development.

NSAIDs, are highly bound to HSA, although lacking the carboxylic moiety. To explore the relationships between physicochemical (VOLSURF) and specific 3D-pharmacophoric descriptors (ALMOND) to HSA, a chemometric 3D-QSPR model has been derived.²³ The chemical interpretation of the final model strongly supports the hypothesis of a common binding region between NSAIDs and 2-(*R*)-phenylpropionamides in site II of HSA. The 3D-QSPR model will prove useful in designing a second generation of optimized CXCL8 inhibitors with the desired HSA binding affinity and be helpful to the prioritization of structurally related chemical libraries. Due to the lack of structural information, this combined molecular docking/3D-QSPR approach might help to provide additional information about drugs binding to site II of HSA.

Materials and Methods

Database. The training set includes 37 drug and druglike compounds extracted from three different chemical families. More specifically, it is formed by 10 novel CXCL8 inhibitor compounds (**1–10** in Chart 1), 17 structural analogues of diflunisal²⁴ (**11–27** in Chart 1), and 10 classical NSAIDs²⁵ (**28–37** in Chart 1). The test set includes seven compounds (**38–44** in Chart 2) with different biological activity but with a close structural relationship to the compounds of the training set.²⁵

Protein Binding Determination. The human protein binding for 10 CXCL8 inhibitors (**1–10** in Chart 1) was experimentally determined as described in the Experimental Section. The HSA binding constant affinity K_i was calculated for **1–10** and **28–44** according to eq 1¹⁴

$$\log K_i = \log \frac{fb}{1 - fb} - \log [\text{HSA}] \quad (1)$$

where K_i is a measure of binding affinity to HSA, under the assumption that the binding to plasma proteins occurs mostly to HSA, fb represents the drug fraction bound to plasma proteins; the concentration of albumin ([HSA]) is fixed to 0.6 mM. The fb values for compounds **1–10** were experimentally determined, whereas fb for **28–44** were obtained from Goodman and Gilman's handbook and from the literature.^{14,25} Moreover, the binding constant affinity for compounds **11–27** was derived from literature data.²⁴

The 2D chemical structures of the training set and test set compounds are respectively shown in Charts 1 and 2, whereas the corresponding $\log K_i$ values are listed in Tables 1 and 2.

Chemistry. 2-(*R*)-Phenylpropionamides (**1–10** in Chart 1) were prepared starting from optically pure 2-(*R*)-phenylpropionic acids following well-established procedures for the preparation of amides (see Experimental Section).

Computational Approach. All calculations were accomplished using a Linux workstation, under the Fedora operating system. The molecular structures were drawn and geometrically optimized using SYBYL software with the Powell method, within the standard TRIPOS force-field.²⁶ The conformational analysis was performed by the CONFORT procedure fixing the energy level to 20 kcal/mol.²⁷ Molecular docking was performed by GRID-GLUE software.²⁸ The molecular

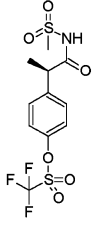
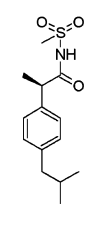
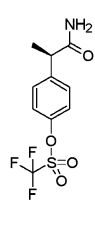
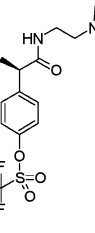
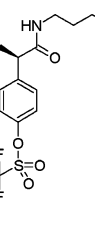
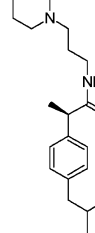
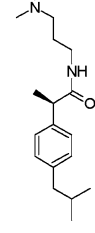
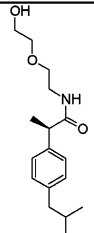
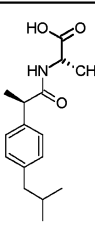
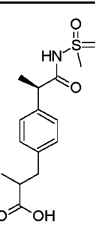
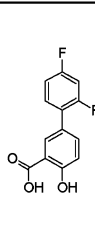
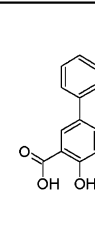
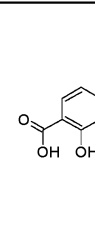
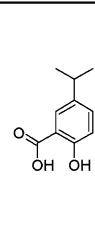
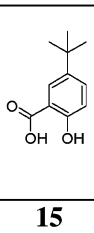
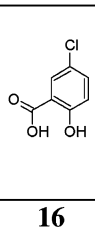
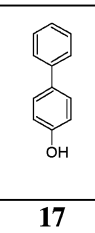
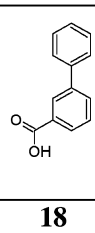
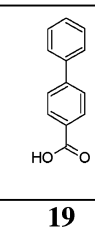
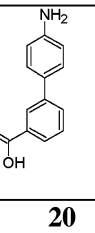
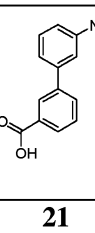
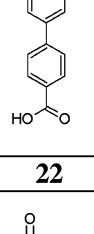
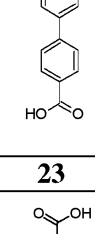
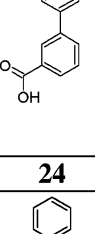
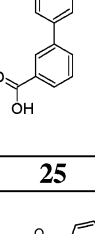
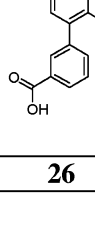
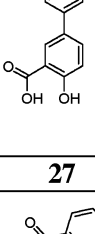
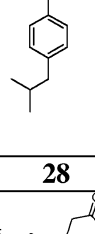
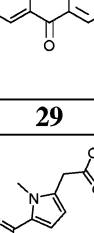
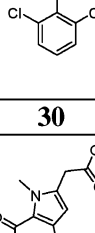
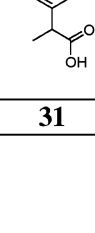
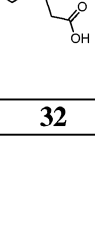
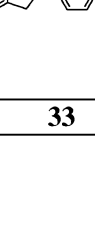
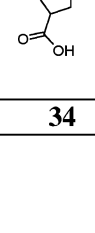
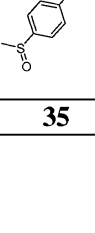
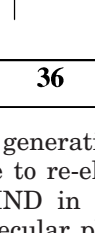
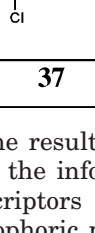
descriptors calculation was made using VOLSURF²⁹ and ALMOND³⁰ software. Finally, the statistical model was generated using GOLPE software.³¹

Molecular Docking. Molecular docking was performed on all the training set molecules, using the flexible protein–ligand option in the GRID–GLUE procedure.²⁸ GLUE is a docking tool that uses the GRID force field to locate the ligand inside the protein cavity. A new algorithm evaluates the protein–ligand interactions and selects the most favorable ligand torsion angles to maximize protein–ligand interactions. To study the HSA sites I and II, 3D crystal structures of HSA complexed with warfarin⁶ (PDB code 1h9z)³² and complexed with propofol¹⁰ (PDB code 1e7a)³² have been used as starting models.

Physicochemical Descriptors. VOLSURF is a molecular modeling software that generates 2D molecular descriptors from the 3D molecular interaction field (MIF) on GRID maps.²⁹ The basic idea of VOLSURF is to compress the information contained in 3D maps calculated by GRID into a few 2D numerical descriptors, which show the great advantage of a simple chemical interpretation. GRID is a computational procedure for the determination of energetically favorable binding sites between a probe and all the atoms in a molecule virtually inserted in a 3D GRID map.^{28,33} The probe is chosen in a variety of chemical groups that are supposed to interact with the molecule. The GRID force field uses a potential based on the total energy of interaction (the sum of Leonard-Jones, H-bonding, electrostatic, and hydrophobic terms) between a target molecule and a probe to characterize putative polar or hydrophobic interactions sites around target molecules.^{28,33} GRID may be used to study small molecular weight molecules, such as drugs, or biological macromolecules.^{33,34} VOLSURF descriptors calculate the principal molecular physicochemical properties and are specifically designed for the optimization of in silico pharmacokinetic properties for pharmaceutically relevant compounds.^{35–37} In this work, VOLSURF calculation produced 94 descriptors (grid spacing 0.5 Å) using three probes to represent potentially important groups in the putative binding site: the water probe (OH2) simulating the solvation–desolvation process, the hydrophobic probe (DRY) computing the hydrophobic energy, and the carbonyl oxygen probe (O) representing the hydrogen-bond acceptors. The DRY probe is a specific probe to compute the hydrophobic energy that can be estimated by means the computation of three terms: the Lennard-Jones potential (that includes stacking, induction, and dispersion interactions with a maximum around -2.0 kcal/mol), the entropic (about -0.8 kcal/mol) and hydrogen-bonding contributions.²⁸

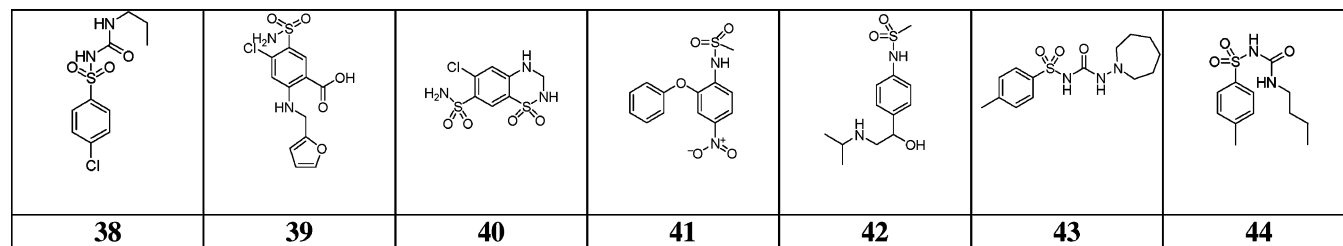
3D-Pharmacophoric Descriptors. ALMOND is a program specifically developed for generating and handling a novel type of molecular descriptor called GRIND (*grid independent descriptors*), based on 3D MIF (calculated by GRID) around a ligand and based on pharmacophoric concepts.^{30,38} GRIND are derived in such a way as to be highly relevant for describing biological properties of compounds while being alignment-independent, chemically interpretable, and easy to compute.³⁸ ALMOND is a program developed for the computation, analysis, and interpretation of GRIND and for

Chart 1. Chemical Structures of the Training Set ($n = 37$).

						
1	2	3	4	5	6	7
						
8	9	10	11	12	13	14
						
15	16	17	18	19	20	21
						
22	23	24	25	26	27	28
						
29	30	31	32	33	34	35
						
36	37					

the generation of the resulting model.³⁰ ALMOND is able to re-elaborate the information contained in the GRIND in 2D descriptors strictly correlated to the molecular pharmacophoric properties.³⁰ In this work, ALMOND computation produced 510 descriptors (grid-spacing 0.5 Å) using the DRY probe, the O probe, the molecular shape probe (TIP), and the amide nitrogen probe (N1) representing the hydrogen-bond donors.

Global Model: Data Matrix. GOLPE is a powerful tool for handling 3D-QSPR problems and improving the quality of the results of a multivariate regression analysis.³¹ GOLPE contains an advanced variable selection procedure, aimed to obtain a PLS model with highest prediction ability.^{39,40} In our chemometric study, GOLPE was used to obtain a global statistical model able to correlate the physicochemical and pharmaco-

Chart 2. Chemical Structures of the Test Set Compounds ($n = 7$).**Table 1.** $\log K_i$ Values for Dataset Compounds

compd	$\log K_i$	SD ^a	PB	SD ^b	compd	$\log K_i$	SD ^a	PB	SD ^b
1	5.92	0.09	99.8		2	6.22	0.03	99.9	
3	4.28	0.05	92.0		4	3.59	0.02	70.0	
5	3.43	0.03	62.0		6	3.98	0.02	85.1	
7	3.70	0.03	75.1		8	3.91	0.08	83.1	
9	4.60	0.01	96.0		10	3.59	0.02	70.2	
11	4.77	0.10			12	5.00	0.09		
13	3.77	0.13			14	4.42	0.19		
15	4.31	0.12			16	4.33	0.16		
17	3.98	0.12			18	5.40	0.33		
19	5.30	0.09			20	3.79	0.07		
21	3.89	0.04			22	3.00			
23	3.00				24	3.76	0.06		
25	3.49	0.11			26	4.38	0.02		
27	3.44				28	5.22		99	
29	5.32		99.2	0.1	30	5.52		99.5	
31	5.52		99.5		32	4.18		90	
33	4.91		98	0.04	34	5.32		99.2	0.1
35	4.42		94	1	36	5.62		99.6	0.1
37	5.04		98.5						

^a Standard deviation (SD) associated with $\log K_i$ ($\log K_i \pm SD$).^b Standard deviation (SD) of the percentage plasma protein binding data (PB \pm SD), from refs 14 and 25.**Table 2.** $\log K_i$ Values for Test Set Compounds

compd	$\log K_i$	PB	SD ^a	compd	$\log K_i$	PB	SD ^a
38	4.60	96.0	0.6	42	2.55	17.5	
39	5.14	98.8	0.2	43	4.73	97	
40	3.36	58	17	44	4.60	96	1
41	4.18	90					

^a Standard deviation (SD) of the percentage plasma protein binding data (PB \pm SD) found in the literature (from refs 14 and 25).

phoric descriptors of the analyzed compounds with HSA binding affinity. PLS analysis was performed in the global X-matrix data represented from the VOLSURF and the ALMOND descriptors; the Y-matrix includes the $\log K_i$ value for each object of the data set.^{41,42} The two blocks of variables were scaled by means of the BUW (block unscaled weights) scaling procedure as implemented in GOLPE software.³¹ This operation separately scales each variable block, whereas the relative scales of single variables within each block remain unchanged. The effect of the BUW procedure is to normalize the scaling of the blocks, thus giving the same importance to each of them. The obtained model was validated by random groups and leave-one-out procedures.³¹

Results and Discussion

The plasma protein binding has been experimentally determined for the CXCL8 inhibitors (shown in Table 1). Binding of **2** to plasma protein has been thoroughly investigated in different animal species. At the concentration of 50 μ M, the unbound drug fraction in human plasma is extremely low (0.1%); further studies have

Table 3. PLS Statistical Results

PC	r^2	q^{2a}	q^{2b}	PC	r^2	q^{2a}	q^{2b}
1	0.69	0.54	0.51	4	0.94	0.62	0.59
2	0.84	0.65	0.61	5	0.96	0.58	0.57
3	0.90	0.67	0.63				

^a Leave one out (LOO). ^b Random groups.

demonstrated that its protein binding is mainly due to the high affinity for HSA, whereas only a very low fraction binds α 1-acid glycoprotein (data not shown).

HSA being the most abundant protein in human plasma, it has been assumed that the binding of drugs occurs mostly to HSA.

Molecular docking analysis supports the hypothesis that site II of HSA is a preferential binding site for most of the compounds in the data set. As assessed by direct binding energy comparison (data not shown), the binding preference to site II is strongly accentuated for the molecules in the data set with an high value of $\log K_i$ (Table 1). In agreement with the literature data, all NSAIDs were selective ligands for site II. Similarly, most of diflunisal analogues were selective ligands for site II, excepting the weak binders **20**, **21**, **22**, **23**, and **27**, which show some propensity to bind site I. Finally, the 10 CXCL8 inhibitors were preferential ligands for site II with poor affinity for site I.

According to the proposed models, all the compounds in the training set engage extensive interactions with hydrophobic residues in the site II pocket (Leu453, Ile388, Asn391, Leu407). Furthermore, electrostatic and hydrogen-bond interactions with specific amino acids of site II, including the backbone of Leu430 and several residues (Tyr411, Arg410, and Ser489), seem crucial in determining the HSA site II binding affinity.

Chemometric analysis of the X-matrix data gave a statistically significant model without any outlier behavior; Table 3 shows the statistical values of the PLS model obtained with five principal components.

The PLS $T-U$ plot in Figure 1 (panel a) represents the trend of all the modeled objects. The points in the upper part of the plot represent the compounds with major HSA binding affinity, whereas those in the lower part represent the compounds with lower affinity.

The PLS score plot in Figure 1 (panel b), representing the positions of X-matrix objects in the multidimensional descriptor space, shows the correlation between the X descriptors and the Y-dependent variable for each component. The first component is, by far, the most informative and reports the main correlation between HSA binding affinity and structural descriptors. The three lines drawn in Figure 1 (panel b) graphically identify three regions of HSA binding affinity: high affinity, intermediate affinity, and low affinity.

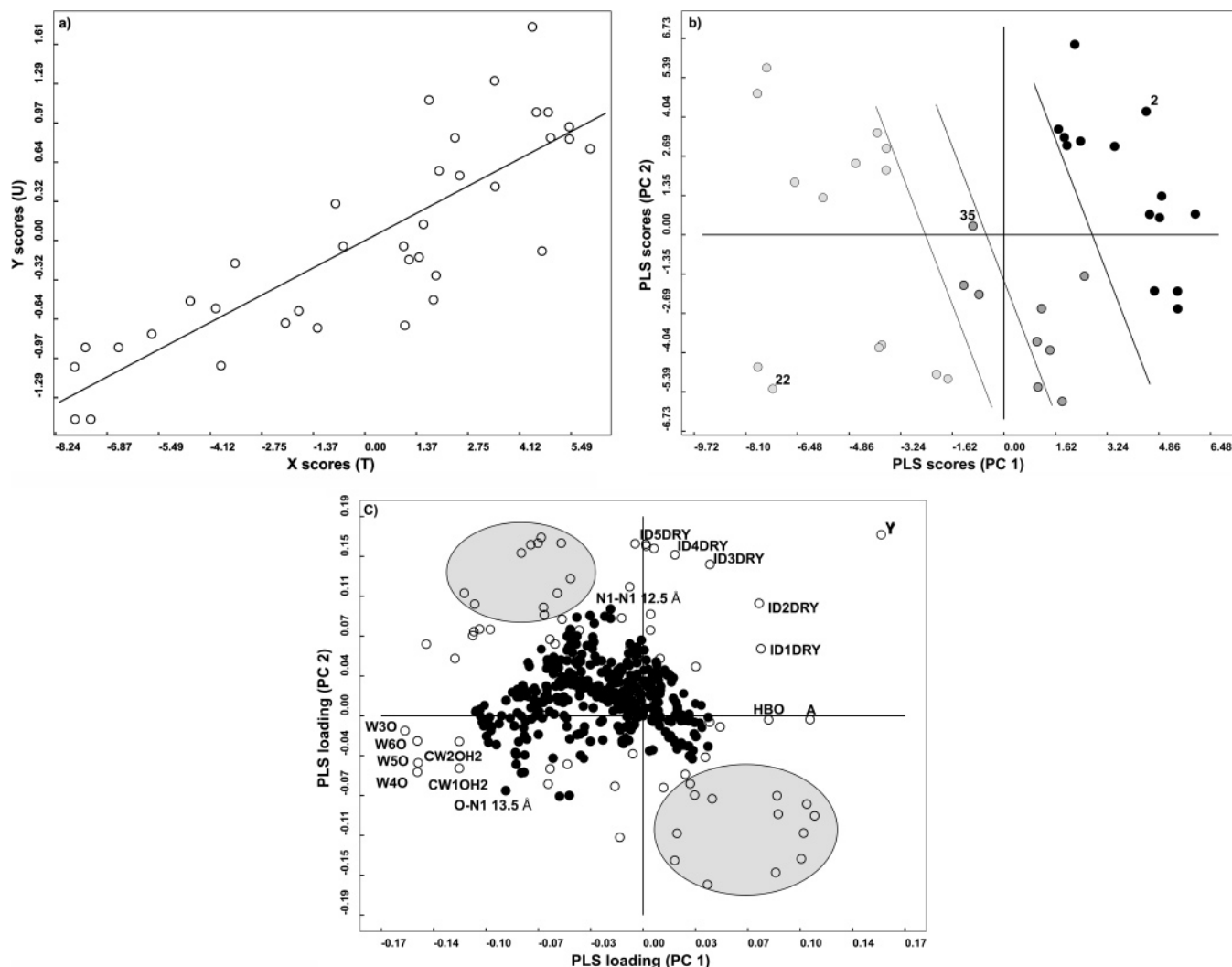


Figure 1. (a) PLS $T-U$ plot for compounds reported in Table 1. Circles depicted in the upper part of the plot represent compounds with high HSA binding affinity; circles in the central part of the plot represent the compounds with intermediate affinity; circles in the lower part represent compounds with low HSA binding affinity. (b) PLS score plot (first versus second component) for the global model. The three lines graphically identify three distinct regions of HSA binding affinity as described above. The model offers a good discrimination between compounds with high HSA binding affinity (black circles on the right of the plot), medium affinity (dark gray circles in the center), and low affinity (light gray circles on the left of the plot). Compounds **2**, **35**, and **22** are visualized respectively as high, intermediate, and low HSA binders. (c) PLS loading plot for the global model. Open circles represent the physicochemical molecular descriptors (VOLSURF); filled circles represent the 3D-pharmacophoric descriptors (ALMOND). HSA binding affinity increases with the relative increase of the hydrophobic integrity moment at five energy levels (IDDRY), hydrogen-bonding capability (HBO), and amphiphilic moment (A); conversely, it decreases when capacity factor values (CW) at two energy levels increase and hydrophilic regions at four different energy levels (W) become larger. The right-lower ellipse includes the VOLSURF descriptors IWOH2, DIFF, and BV, and the left-upper ellipse includes the VOLSURF descriptors VOH2, SOH2, GOH2, POL, MW, and EEFR as described in the text. Moreover, the HSA binding increases when in the target hydrogen donor groups are present at about 12.5 Å distance; conversely it decreases when hydrogen acceptor/donor groups are present at about 13.5 Å.

The high affinity ligand (right region) cluster contains three CXCL8 inhibitors (**1**, **2**, **9**), three diflunisal analogues (**12**, **18**, **19**), and most of the NSAIDs compounds (**28–31**, **33**, **34**, **36**, **37**).

The intermediate affinity ligand (central region) cluster contains one CXCL8 inhibitor (**3**), some diflunisal analogues (**11**, **14–17**, **26**), and two NSAIDs (**32**, **35**).

The low affinity ligand (left region) cluster comprises some CXCL8 inhibitors (**4–8**, **10**) and most of the diflunisal analogues (**13**, **20–25**, **27**).

The loading plot of Figure 1 (panel c) represents the contribution of original variables to the latent variables. VOLSURF and ALMOND descriptors are reported with different symbols.

It is clear that the physicochemical descriptors (VOLSURF) are more directly related to the HSA binding than the 3D-pharmacophoric ones (ALMOND). The statistical comparison shows that the physicochemical descriptors account for 50% of the HSA binding whereas the 3D-pharmacophoric ones account for 30% of the HSA affinity.⁴³ It is important to stress that it is the balance of all descriptors which controls HSA binding affinity. Table 4 lists some of the most important VOLSURF descriptors and their definitions.²⁹

A careful analysis of the loading plot shows that HSA binding affinity increases with the relative increase of the hydrophobic integrity moments, calculated at five different energy levels (IDDRY), hydrogen-bonding capability (HBO), and amphiphilic moment (A); conversely

Table 4. Definition of Several VOLSURF Physicochemical Descriptors

Volsurf 2D descriptors
IDDRY (hydrophobic integrity moment) measures the unbalance between the center of mass of molecules and the position of the hydrophobic regions around them, calculated at eight energy levels by hydrophobic probe DRY. Integrity moments are vectors pointing from the center of the mass to the center of the hydrophobic regions.
HBO (hydrogen bonding) measures of the hydrogen-bonding capability calculated by O probe.
A (amphiphilic moment) is defined as a vector pointing from the center of the hydrophobic domain to the center of the hydrophilic domain.
CWOH₂ (capacity factors) represents the ratio between the hydrophilic regions and the molecular surface calculated by water probe.
W (hydrophilic regions at eight energy levels) may be defined as the molecular envelope accessible by solvent water molecules.
IWOH₂ (hydrophilic integrity moment) measures the unbalance between the center of the mass of molecules and the position of the hydrophilic regions around them calculated by water probe at eight energy levels.
DIFF (diffusivity) measures the molecular diffusivity in water at 25 °C.
BV (best volume) identifies the largest volumes of hydrophilic (BVOH ₂) or hydrophobic regions (BVDRY) in the molecular structures.
VOH₂ (molecular volume) is defined when a water probe is interacting with a target solute molecule. It represents the water solvent excluded volume (in Å ³) or the volume contained within the water accessible surface computed at 0.20 kcal/mol.
SOH₂ (molecular surface) is defined when a water probe is interacting with a target solute molecule. It represents the accessible surface (in Å ²) traced out by a water probe interacting at 0.20 kcal/mol when it rolls over the target molecule.
GOH₂ (molecular globularity) defined by the ratio Surface/Sequiv, in which Sequiv is the surface area of a sphere of volume V.
POL (molecular polarizability) is an estimation of the average molecular polarizability.
MW (molecular weight).
EEFR (elongation/fixated elongation) refers to the maximum extension a molecule could reach if properly stretched. The two descriptors are
elongation , the most probable extension of the molecule;
fixated elongation , the portion of the extension given by the rigid part of a molecule.

it decreases when best volume (BV) values increase and hydrophilic regions at four different energy levels (W) become larger. The following conclusions can be drawn by the analysis of the results: VOLSURF descriptors of hydrophilic interactions, such as hydrophilic regions (W), are inversely correlated with HSA binding; on the contrary, VOLSURF descriptors of hydrophobic interactions, such as hydrophobic integrity moment (IDDRY), are directly correlated with HSA binding affinity. Hence, hydrophilic regions are detrimental for drug interaction with albumin. However, the presence of concentrated hydrophobic regions, located opposite to regions with high capability to engage hydrogen bonds with the target, strongly favors the binding to site II of HSA.

In the loading plot of Figure 1 (panel c), two additional blocks of VOLSURF descriptors (Table 4) directly related to the HSA binding are highlighted. The first group is located in the lower right ellipse of the loading plot and includes molecular physicochemical descriptors with a positive absolute value on the first component and negative absolute value on the second component of the model (DIFF, IWOH₂, BV). The second group is located in the upper left ellipse of Figure 1 (panel c) and includes molecular physicochemical descriptors with negative coefficients on the first component and positive on the second component of the PLS model (VOH₂, SOH₂, POL, GOH₂, MW, EEFR). Although both these groups of descriptors clearly influence HSA binding affinity, their orthogonal arrangement in the 3D-space makes the global impact on HSA binding weak.

To clarify the model interpretation, Figure 2 (panels a–c) shows a visual comparison of the 3D MIFs calculated with the DRY probe at about –0.4 kcal/mol for three compounds (**2**, **35**, **22**) respectively selected as strong, intermediate, and weak HSA binders. The contoured zones around the molecules represent the hydrophobic regions interacting with the DRY probe; the red vectors represent the hydrophobic integrity moments (IDDRY) calculated at eight energy levels as reported in Table 4. The size and volume of the hydrophobic regions of **2** are larger than those of **35** and

22; this characteristic, joined with long integrity moment vectors, accounts for the high affinity of **2**. **35**, which is not characterized by diffused hydrophobic regions and whose integrity moment vectors are intermediate long, is a moderate site II binder. Hydrophobic regions in **22** are very restricted and its integrity moment vector is very short; for these reasons **22** is a weak HSA site II substrate.

The loading plot in Figure 1 (panel c) also shows that binding to HSA increases when specific pharmacophoric groups are present at certain distances. When two hydrogen-acceptor groups of the ligand interacting with the hydrogen-donor groups in the target are at about 12.5 Å distance, the binding to HSA increases. This requirement is satisfied in all the best HSA ligands in the database. Conversely, binding affinity decreases when hydrogen-acceptor-donor groups in the target at about 13.5 Å are present. The strong effect of acceptor groups on the ligands suggests that the binding with site II occurs through hydrogen bonds with Leu430 (backbone), Arg410, Tyr411, and Ser489 residues in the binding cavity of HSA site II. The precise orientation of hydrogen-bond-donor groups on the target resulting a crucial factor for an optimal HSA site II targeting. Indeed, docking calculations highlight the presence at 12.5 Å distance, in the binding cavity of HSA site II, of Arg410 and Leu430. These specific residues engage hydrogen bonds with carbonylic or sulfonylic oxygen acceptor atoms, present in high-affinity ligands for site II of HSA.

Figure 2 (panels d–f) shows a visual comparison for the MIFs obtained using the N1 probe for **2**, **35**, and **22**. Only **2** features the two hydrogen-bond acceptor (connected by the red line) at 12.5 Å distance, whereas the same features in **35** and **22** are clearly more distant.

Summarizing, the evaluation of hydrophobic regions and integrity moment values, combined with the analysis of specific pharmacophoric points, allows the identification of high-affinity ligands for HSA site II.

Validation Model. The evaluation of the predictive capability of the developed PLS model has been carried

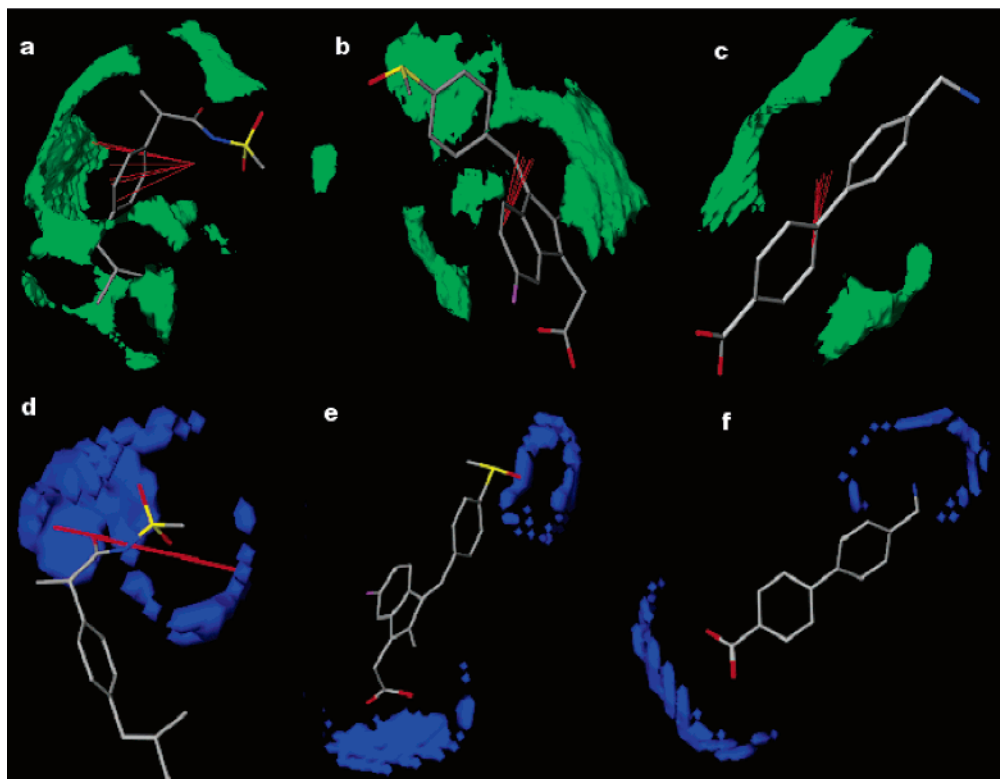


Figure 2. (a, b, c) Comparison of the 3D MIFs calculated by use of the DRY probe among **2**, **35**, and **22**. The areas surrounding these molecules represent the hydrophobic regions interacting with the DRY probe contoured at -0.4 kcal/mol; the red vectors represent the hydrophobic integrity moment (IDDRY) calculated at eight energy levels. (d, e, f) Comparison of the 3D MIFs calculated by using N1 probe among **2**, **35**, and **22**. The areas surrounding the molecules represent regions interacting with the N1 probe and able to accept hydrogen bonds. The red line emerging in **2** represents the pharmacophoric distance of 12.5 Å, which is essential to enhance the HSA affinity.

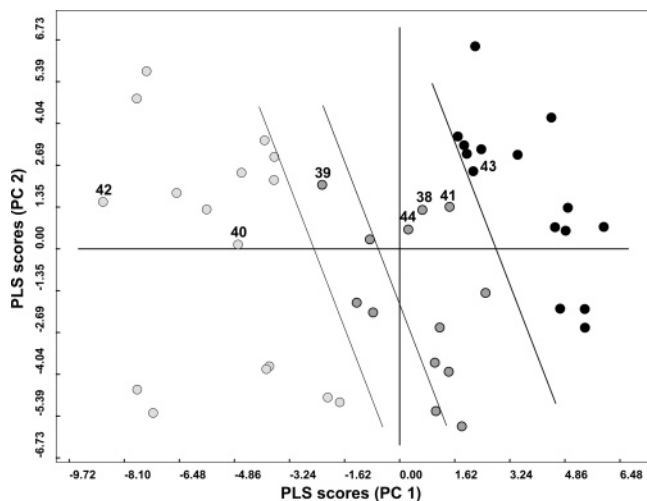


Figure 3. PLS score prediction plot: the shown external test set molecules are projected on the global PLS model of Figure 1b. From a visual inspection of the plot, all the external compounds are correctly predicted by the model (see text).

out for seven test set molecules selected from literature data.^{14,25} The molecular structures and the experimental binding data are respectively reported in Chart 2 and Table 2. The quality of the external prediction is graphically shown in the PLS score plot of Figure 3 in which these compounds are projected into the model. The three lines graphically highlight the three regions of HSA binding affinity: high (right), intermediate (center), and low (left) binding affinity regions. This plot

shows that prediction of the test set is in good agreement with the experimental data (see Table 2). In fact, **43** is located in the high binding affinity region; **38**, **39**, **41**, **44** are predicted in the intermediate affinity region, whereas **40** and **42** are projected into the low binding affinity region (Figure 3). The prediction ability of the developed PLS model was demonstrated by the correct prediction for this external test set, confirming the quality and the statistical significance of the PLS model.

Conclusions

Plasma protein binding dramatically influences both the pharmacokinetic and the pharmacodynamic profile of potential drug candidates but, to date, only a limited number of *in silico* models for the evaluation of drug-binding affinity to HSA have been reported. A novel class of CXCL8 inhibitors showed an extremely high affinity toward HSA. With the aim of guiding the design of second-generation leads with reduced protein binding, a chemometric 3D-QSPR approach was used to model HSA binding affinity. Due to the structural similarity between CXCL8 inhibitors and classical NSAIDs, a preferential binding to site II was assumed.

A preliminary molecular docking was performed on all the training set molecules to estimate their binding affinity for sites I and II of HSA. This approach confirmed that the most of the molecules in the training set are preferential ligands for site II. On the basis of this assumption, a good statistical model was developed that was able to describe the drug HSA site II interaction in a quantitative manner.

The global PLS model examined the impact on HSA binding of physicochemical molecular properties as well as of pharmacophoric properties. The quantitative relationship between 3D-structure and HSA binding affinity to site II was discussed. Hydrophilic regions are detrimental for drug interaction with HSA, whereas the presence of concentrated hydrophobic regions, located opposite to the hydrogen-bond-acceptor groups, strongly favor HSA binding. Moreover, specific pharmacophoric points distancing about 12.5 Å are important to enhance the affinity for site II of HSA. Finally, the good prediction ability of the PLS model was demonstrated by the correct prediction for external test molecules. Accordingly, on the basis of the model, novel optimized CXCL8 inhibitors could be designed with the desired HSA binding affinity. All these results suggest that the chemometric strategies described in this paper might be a powerful tool in pharmaceutical industries to optimize ADME properties of lead compounds, during the early phase of drug discovery.

Experimental Section

General Experimental Procedures. Optical rotations were measured on a Perkin-Elmer 241 polarimeter and the $[\alpha]^{25}_D$ values are given in 10^{-1} deg $\text{cm}^2 \text{g}^{-1}$. ^1H NMR spectra were recorded on a Bruker ARX 300 spectrometer. Melting points were determined using a Büchi capillary melting point apparatus and are uncorrected. Elemental analyses were within $\pm 0.4\%$ of the theoretical values calculated for C, H, and N and are reported only with symbols.

All reagents and solvents were purchased from Sigma-Aldrich or Lancaster and used without further purification. Reaction courses and product mixtures were monitored by thin-layer chromatography on silica gel (precoated F₂₅₄ Macherey-Nagel plates); the spots were examined with UV light and visualized with I₂.

The HPLC–UV analysis was carried out using a chromatographic system composed by a Model 2690 pump, a Model 486 UV–vis detector (Waters, Milford, MA), and a Model 7725i sample injector (Rheodyne, Cotati, CA) equipped with a 20- μL loop. Chromatographic data management was automated using Millennium³² software (Waters, Milford, MA).

The HPLC–fluorescence analysis was carried out using the same chromatographic system above-described equipped with a Model 474 scanning fluorescence detector (Waters, Milford, MA).

The HPLC–MS/MS analysis was carried out using a Model Surveyor MS pump, a Model Surveyor AS sample injector, and a Model LCQ Deca XP Plus MSⁿ ion trap mass spectrometer (Thermo Finnigan, San Jose, CA). Chromatographic data management was automated using a software Xcalibur Instrument Control, (Thermo Finnigan, San Jose, CA).

Protein Binding Determination in Human Plasma. The *in vitro* binding of CXCL8 inhibitors to human plasma proteins was investigated by ultrafiltration using the Centrifree micropartition system. Separation of free compound from protein-bound material was achieved by filtration of the sample through an ultrafiltration membrane.^{44–46}

Duplicate drug-free plasma samples were mixed with each CXCL8 inhibitor under investigation at the nominal concentration of 20 $\mu\text{g}/\text{mL}$ and incubated at 37 °C for 20 min. The spiked plasmas were subsequently transferred to ultrafiltration units, which were centrifuged at 1500 rpm for about 15 min. The degree of test article binding to the apparatus, or nonspecific binding, was assessed by investigating the ultrafiltration of sodium phosphate buffered saline spiked with the analytes at 20 $\mu\text{g}/\text{mL}$, in the same manner.

The unbound test article in the obtained ultrafiltrates was quantified by reversed phase HPLC analysis with UV, fluorescence, or MS/MS detection, depending on the nature of the molecule, using the following expressions:

$$\% \text{ free fraction} = \frac{\text{area of filtered sample}}{\text{area of unfiltered sample}} \times 100$$

$$\% \text{ protein binding} = 100 - \% \text{ free fraction}$$

Chromatographic separations were performed at room temperature. Analytical columns, mobile phases, detection conditions, injected volumes, and flow rates together with typical retention times are reported in Table 5. The selected chromatographic conditions were suitable for good resolution between the analytes of interest and the plasma ultrafiltered endogenous peaks.

Chemistry. Synthesis of (*R*)-2-Arylpropionic Acids Intermediates. (*R*)-2-(4-Isobutylphenyl)propionic Acid.

The optical resolution of the racemic acid was performed as described.⁴⁷ (*R*)-2-(4-Isobutylphenyl)propionic acid (50 g, 35%) was obtained as a white solid: mp 48–49 °C; $[\alpha]^{25}_D$ ($c = 2$, EtOH) -53° ; ee = 98%; HPLC–UV, Chiralcel OD column, 500:5:0.5 *n*-hexane:PrOH:AcOH, $t_R = 13.8$ min; ^1H NMR (CDCl_3) δ 7.15 (d, 2H, $J = 7$ Hz), 6.95 (d, 2H, $J = 7$ Hz), 3.58 (q, 1H, $J = 7$ Hz), 2.30 (d, 2H, $J = 7$ Hz), 1.75 (m, 1H), 1.35 (d, 3H, $J = 7$ Hz), 0.85 (d, 6H, $J = 7$ Hz). Anal. ($\text{C}_{13}\text{H}_{18}\text{O}_2$) C, H, N.

(*R*)-2-(4-Hydroxyphenyl)propionic Acid. The optical resolution of the racemic acid was performed as described.⁴⁷ (*R*)-2-(4-Hydroxyphenyl)propionic acid (34.7 g, 29%) was obtained as a white solid: mp 156–158 °C; $[\alpha]^{25}_D$ ($c = 1$, MeOH) -72° ; ee = 97%; HPLC–UV, Chiralcel OJ column, 75:15:10 *n*-hexane:EtOH:PrOH and 0.5% trifluoroacetic acid, $t_R = 10.95$ min; ^1H NMR (CDCl_3) δ 7.12 (d, 2H, $J = 7$ Hz), 6.75 (d, 2H, $J = 7$ Hz), 5.45 (s, 1H, OH), 3.62 (q, 1H, $J = 7$ Hz), 1.45 (d, 3H, $J = 7$ Hz). Anal. ($\text{C}_9\text{H}_{10}\text{O}_3$) C, H, N.

(*R*)-2-(4-Hydroxyphenyl)propionic Acid Methyl Ester.

HCl (37%, 5 mL) was added to a solution of (*R*)-2-(4-hydroxyphenyl)propionic acid (34.7 g, 0.21 mol) in methanol (450 mL) and, after stirring at rt for 18 h, the solvent was removed under vacuum and the residue taken up with CH_2Cl_2 (250 mL). The organic phase was washed with water and with a saturated solution of NaHCO_3 and dried over Na_2SO_4 , to give, after solvent evaporation, pure (*R*)-2-(4-hydroxyphenyl)propionic acid methyl ester (35.2 g, 93%) as a slightly yellow oil: ^1H NMR (CDCl_3) δ 7.18 (d, 2H, $J = 7$ Hz), 6.82 (d, 2H, $J = 7$ Hz), 5.7 (bs, 1H, CONH), 3.70 (s, 3H), 3.65 (q, 1H, $J = 7$ Hz), 1.52 (d, 3H, $J = 7$ Hz). Anal. ($\text{C}_{10}\text{H}_{12}\text{O}_3$) C, H, N.

(*R*)-2-(4-Trifluoromethanesulfonyloxyphenyl)propionic Acid Methyl Ester.

A solution of (*R*)-2-(4-hydroxyphenyl)propionic acid methyl ester (35 g, 0.19 mol) and *N,N*-diisopropylamine (39 mL, 0.23 mol) in CH_2Cl_2 (170 mL) at -15 °C was treated, under inert atmosphere, with trifluoromethanesulfonic anhydride (38.7 mL, 0.23 mol). At the end of the adding, the mixture was left stirring for 3 h at rt. The organic solution was washed with water (3×250 mL) and, after drying with Na_2SO_4 , solvent was removed under vacuum to give (*R*)-2-(4-trifluoromethanesulfonyloxyphenyl)propionic acid methyl ester (56.4 g, 95%) as a brown oil: ^1H NMR (CDCl_3) δ 7.45 (d, 2H, $J = 7$ Hz), 7.21 (d, 2H, $J = 7$ Hz), 3.85 (q, 1H, $J = 7$ Hz), 3.65 (s, 3H), 1.50 (d, 3H, $J = 7$ Hz). Anal. ($\text{C}_{11}\text{H}_{11}\text{F}_3\text{O}_5\text{S}$) C, H, N.

(*R*)-2-(4-Trifluoromethanesulfonyloxyphenyl)propionic Acid.

(*R*)-2-(4-Trifluoromethanesulfonyloxyphenyl)propionic acid methyl ester (56 g, 0.18 mol) was dissolved in a solution of glacial acetic acid (330 mL) and 37% HCl (57 mL) and refluxed for 3 h. After cooling at rt the residue was dissolved in CH_2Cl_2 (200 mL) and washed with water (3×250 mL). After drying over Na_2SO_4 , solvent was removed under vacuum to give (*R*)-2-(4-trifluoromethanesulfonyloxyphenyl)propionic acid (44.5 g, 83%) as a white solid: mp 57–60 °C; $[\alpha]^{25}_D$ ($c = 1$, MeOH) -32° ; ^1H NMR (CDCl_3) δ 7.54 (d, 2H, $J = 7$ Hz), 7.25 (d, 2H, $J = 7$ Hz), 3.85 (q, 1H, $J = 7$ Hz), 1.58 (d, 3H, $J = 7$ Hz). Anal. ($\text{C}_{10}\text{H}_9\text{F}_3\text{O}_5\text{S}$) C, H, N.

Synthesis of CXCL8 Inhibitors. (*R*)-2-(4-Trifluoromethanesulfonyloxyphenyl)-*N*-methanesulfonylpropionamide (1).

1,1'-Carbonyldiimidazole (7.21 g, 44.5 mmol) was added to a solution of (*R*)-2-(4-trifluoromethanesulfonyloxyphenyl)propionic acid (13.28 g, 44.5 mmol) in dry CH_2Cl_2 (130 mL), and the resulting mixture was left stirring at rt for

Table 5. Chromatographic Conditions for Human Protein Binding Determination

analyte	mobile phase	detection	injected vol (μ L)	analytical column	flow rate (mL/min)	t_R (min)
1	0.05 M KH_2PO_4 (pH 3): $\text{CH}_3\text{CN}:\text{CH}_3\text{OH}$, 40:25:35	UV, 215 nm	20	Hypersil BDS C18, 250 \times 4 mm, 5 μ m (Thermo Hypersil)	1.0	6.3
2	0.02 M NH_4HCOO (pH 4.3):MeOH gradient elution (linear), from 30/70 to 20/80 in 3 min	MS/MS, ESI+, m/z : parent 301, daughter 284	10	Luna C18 150 \times 2 mm, 5 μ m (Phenomenex)	0.2	5.8
3	0.05 M KH_2PO_4 (pH 3): $\text{CH}_3\text{CN}:\text{CH}_3\text{OH}$, 40:25:35	UV, 215 nm	20	Hypersil BDS C18, 250 \times 4 mm, 5 μ m (Thermo Hypersil)	1.0	5.5
4	0.05 M KH_2PO_4 (pH 3): CH_3CN , 66:34	UV, 215 nm	10	Luna C18, 250 \times 4.6 mm (Phenomenex)	1.0	6.5
5	0.05M KH_2PO_4 (pH 3): CH_3CN , 66:34	UV, 215 nm	10	Luna C18, 250 \times 4.6 mm (Phenomenex)	1.0	9.5
6	0.05 M KH_2PO_4 (pH 2.5): CH_3OH , 32:68	UV, 223 nm	20	Hypersil BDS C18, 250 \times 4 mm, 5 μ m (Thermo Hypersil)	1.0	6.0
7	0.05 M KH_2PO_4 (pH 2.5): CH_3OH , 32:68	UV, 223 nm	20	Hypersil BDS C18, 250 \times 4 mm, 5 μ m (Thermo Hypersil)	1.0	5.4
8	0.05M KH_2PO_4 (pH 3): CH_3CN , 60:40	fluorescence: ex 223 nm, em 288 nm	20	Lichrospher RP 60 Select B, 250 \times 4 mm (Merck)	1.5	6.9
9	0.05 M KH_2PO_4 (pH 3): CH_3CN , 70:30	fluorescence: ex 223 nm, em 287 nm	20	Lichrospher RP 60 Select B, 250 \times 4 mm (Merck)	1.5	9.7
10	0.05 M KH_2PO_4 (pH 3): CH_3OH , 50:50	UV, 223 nm	20	Hypersil BDS C18, 250 \times 4 mm, 5 μ m (Thermo Hypersil)	1.0	5.7

90 min. Methanesulfonamide (4.23 g, 44.5 mmol) and DBU (6.65 mL, 44.5 mmol) were added, and the mixture was left stirring 16 h further at rt. The organic phase was washed with 0.5 N HCl (2 \times 50 mL), 5% NaH_2PO_4 (3 \times 50 mL), and water (2 \times 50 mL). After drying with Na_2SO_4 , solvent was removed under vacuum, and the residue was taken up with *n*-hexane (50 mL) and pulped at rt for 16 h. The formed precipitate was filtered under vacuum and dried in an oven at 50 $^\circ\text{C}$ to give pure **1** as a white powder (13.2 g, 79%): mp 98–100 $^\circ\text{C}$; $[\alpha]_D^{25}$ ($c = 0.5$, MeOH) -49° ; $^1\text{H NMR}$ (CDCl_3) δ 7.40 (d, 2H, $J = 7$ Hz), 7.23 (d, 2H, $J = 7$ Hz), 3.68 (q, 1H, $J = 7$ Hz), 3.15 (s, 3H), 1.42 (d, 3H, $J = 7$ Hz). Anal. ($\text{C}_{11}\text{H}_{12}\text{F}_3\text{NO}_6\text{S}_2$) C, H, N.

***N*-[(*R*)-2-(4-Isobutylphenyl)propionyl]methanesulfonamide (2).** Compound **2** was synthesized (79%) using the same procedure described for **1** starting from (*R*)-2-(4-isobutylphenyl)propionic acid: mp 103–105 $^\circ\text{C}$; $[\alpha]_D^{25}$ ($c = 1$, MeOH) -68° ; $^1\text{H NMR}$ ($\text{DMSO}-d_6$) δ 7.30 (d, 2H, $J = 7$ Hz), 7.09 (d, 2H, $J = 7$ Hz), 3.42 (q, 1H, $J = 7$ Hz), 2.81 (s, 3H), 2.45 (d, 2H, $J = 7$ Hz), 1.55 (m, 1H), 1.32 (d, 3H, $J = 7$ Hz), 0.95 (d, 3H, $J = 7$ Hz). Anal. ($\text{C}_{14}\text{H}_{21}\text{NO}_3\text{S}$) C, H, N.

(*R*)-2-(4-Trifluoromethanesulfonyloxyphenyl)propionamide (3). Thionyl chloride (4.8 mL, 67 mmol) was added to a solution of (*R*)-2-(4-trifluoromethanesulfonyloxyphenyl)propionic acid (10 g, 33.5 mmol) in dry CH_2Cl_2 (130 mL), and the resulting solution was refluxed for 2 h. After cooling at rt, toluene and thionyl chloride were removed under vacuum, and the residue was dissolved in CH_2Cl_2 (25 mL); gaseous ammonia was bubbled into the solution for 1 h. The organic solution was washed with water (2 \times 50 mL), and after drying with Na_2SO_4 , solvent was removed under vacuum and the crude was suspended in *n*-hexane. After stirring at rt for 16 h, pure **3** was isolated by filtration as a white powder (8.1 g, 27.2 mmol, 81%) mp 67–69 $^\circ\text{C}$; $[\alpha]_D^{25}$ ($c = 0.5$, MeOH): -12° ; $^1\text{H NMR}$ (CDCl_3) δ 7.48 (d, 2H, $J = 7$ Hz), 7.22 (d, 2H, $J = 7$ Hz), 5.38 (bs, 2H, CONH_2), 3.65 (q, 1H, $J = 7$ Hz), 1.55 (d, 3H, $J = 7$ Hz). Anal. ($\text{C}_{10}\text{H}_{10}\text{F}_3\text{NO}_4\text{S}$) C, H, N.

(*R*)-2-(4-Trifluoromethanesulfonyloxyphenyl)-*N*-[2-(pyrrolidin-1-yl)ethyl]propionamide (4). Compound **4** was synthesized (75%) using the same procedure described for **3** starting from (*R*)-2-(4-trifluoromethanesulfonyloxyphenyl)propionic acid and 2-(pyrrolidin-1-yl)ethylamine: $[\alpha]_D^{25}$ ($c = 1$, MeOH) -34° ; $^1\text{H NMR}$ (CDCl_3) δ 8.65 (bs, 1H, CONH), 7.75 (d, 2H, $J = 7$ Hz), 7.22 (d, 2H, $J = 7$ Hz), 4.02 (m, 2H), 3.85–3.74 (m, 3H), 3.31 (m, 2H), 3.0–2.85 (m, 2H), 2.41–2.12 (m, 4H), 1.65 (d, 3H, $J = 7$ Hz). Anal. ($\text{C}_{16}\text{H}_{21}\text{F}_3\text{N}_2\text{O}_4\text{S}$) C, H, N.

(*R*)-2-(4-Trifluoromethanesulfonyloxyphenyl)-*N*-[3-(pyrrolidin-1-yl)propyl]propionamide (5). Compound **5** was

synthesized (70%) using the same procedure described for **3** starting from (*R*)-2-(4-trifluoromethanesulfonyloxyphenyl)propionic acid and 3-(pyrrolidin-1-yl)propylamine. $[\alpha]_D^{25}$ ($c = 1$, MeOH) -41° ; $^1\text{H NMR}$ (CDCl_3) δ 8.01 (bs, 1H, CONH), 7.62 (d, 2H, $J = 7$ Hz), 7.15 (d, 2H, $J = 7$ Hz), 3.80 (q, 1H, $J = 7$ Hz), 3.52 (m, 2H), 3.31 (m, 2H), 2.95 (m, 2H), 2.78 (m, 2H), 2.15–1.90 (m, 6H), 1.55 (d, 3H, $J = 7$ Hz). Anal. ($\text{C}_{17}\text{H}_{23}\text{F}_3\text{N}_2\text{O}_4\text{S}$) C, H, N.

(*R*)-2-(4-Isobutylphenyl)-*N*-(1-methylpiperidin-4-yl)propionamide (6). Compound **6** was synthesized (70%) using the same procedure described for **3** starting from (*R*)-2-(4-isobutylphenyl)propionic acid and 1-methyl-4-aminopiperidine: $[\alpha]_D^{25}$ ($c = 0.5$, MeOH) -29° ; $^1\text{H NMR}$ (CDCl_3) δ 7.65 (bs, 1H, CONH), 7.32 (m, 4H), 3.85 (q, 1H, $J = 7$ Hz), 3.75 (m, 1H), 3.52 (m, 2H), 3.15 (m, 2H), 2.91 (s, 3H), 2.50 (d, 2H, $J = 7$ Hz), 2.21–2.05 (m, 2H), 1.95 (m, 1H), 1.80–1.68 (m, 2H), 1.50 (d, 3H, $J = 7$ Hz), 0.95 (d, 6H, $J = 7$ Hz). Anal. ($\text{C}_{19}\text{H}_{30}\text{N}_2\text{O}$) C, H, N.

(*R*)-2-(4-Isobutylphenyl)-*N*-(3-dimethylaminopropyl)propionamide (7). Compound **7** was synthesized (72%) using the same procedure described for **3** starting from (*R*)-2-(4-isobutylphenyl)propionic acid and 3-(dimethylamino)propylamine: $[\alpha]_D^{25}$ ($c = 0.5$, MeOH) -14° ; $^1\text{H NMR}$ (CDCl_3) δ 7.32 (d, 2H, $J = 7$ Hz), 7.15 (d, 2H, $J = 7$ Hz), 6.77 (bs, 1H, CONH), 3.52 (q, 1H, $J = 7$ Hz), 3.35–3.20 (m, 2H), 2.55 (d, 2H, $J = 7$ Hz), 2.22 (t, 2H, $J = 7$ Hz), 2.05 (s, 6H), 1.95 (m, 1H), 1.50 (m, 5H), 1.05 (d, 6H, $J = 7$ Hz). Anal. ($\text{C}_{18}\text{H}_{30}\text{N}_2\text{O}$) C, H, N.

(*R*)-2-(4-Isobutylphenyl)-*N*-[2-(2-hydroxyethoxy)ethyl]propionamide (8). Compound **8** was synthesized (65%) using the same procedure described for **3** starting from (*R*)-2-(4-isobutylphenyl)propionic acid and 2-(2-aminoethoxy)ethanol. $[\alpha]_D^{25}$ ($c = 3$, EtOH) -3.5° ; $^1\text{H NMR}$ (CDCl_3) δ 7.23 (d, 2H, $J = 7$ Hz), 7.13 (d, 2H, $J = 7$ Hz), 5.77 (bs, 1H, CONH), 3.75–3.33 (m, 9H), 2.47 (d, 2H, $J = 7$ Hz), 1.85 (m, 1H), 1.63 (d, 3H, $J = 7$ Hz), 0.94 (d, 6H, $J = 7$ Hz). Anal. ($\text{C}_{17}\text{H}_{27}\text{NO}_3$) C, H, N.

(*S*)-2-[(*R*)-2-(4-Isobutylphenyl)propionylamino]propionic Acid (9). To a solution of (*R*)-2-(4-isobutylphenyl)propionic acid (5 g, 24.24 mmol) in dioxane (10 mL) was added thionyl chloride (2.71 mL, 36.36 mmol), and the resulting solution was heated at reflux for 3.5 h. After cooling at rt the acyl chloride was dissolved in DMF (20 mL) at $T = 0^\circ\text{C}$, and DCC (5 g, 24.24 mmol) and HOBT (3 g, 22.2 mmol) were added under stirring. After 30 min a solution of L-alanine methyl ester hydrochloride (3.2 g, 22.2 mmol) and triethylamine (3 mL) in DMF (5 mL) was added. The resulting mixture was left stirring for 2 h at 0 $^\circ\text{C}$ and overnight at rt. The precipitated DCU was filtered off; the filtrate was diluted with EtOAc (50

mL), and the organic phase was washed with 10% buffer citric acid (2 × 20 mL), with a saturated solution of NaHCO₃ (2 × 20 mL), and then with brine (20 mL). After drying with Na₂SO₄, solvent was evaporated to give a crude product (3.86 g) that was suspended in *n*-hexane (60 mL) and left stirring overnight at rt. (S)-2-[(R)-2-(4-isobutylphenyl)propionylamino]propionic acid methyl ester was isolated by filtration as a white powder (4.9 g, 16.84 mmol). To a solution of the methyl ester in dioxane (9 mL) was added 1 N NaOH (17 mL), and the mixture was left stirring overnight at rt. An ice/water mixture (130 mL) was added and the resulting mixture was acidified with H₂SO₄ concentrated to pH = 2. The aqueous phase was extracted with CH₂Cl₂ (4 × 20 mL), and the collected organic extracts were washed with brine (20 mL), dried over Na₂SO₄, and evaporated under vacuum to give an oily residue. **9** was isolated by crystallization from ethyl ether (30 mL) as a white solid (2.55 g, 38%): mp 125–128 °C; [α]_D²⁵ (c = 1, MeOH) –44°; ¹H NMR (CDCl₃) δ 7.21 (d, 2H, *J* = 7 Hz), 7.12 (d, 2H, *J* = 7 Hz), 5.95 (bs, 1H, CONH), 4.54 (q, 1H, *J* = 7 Hz), 3.62 (q, 1H, *J* = 7 Hz), 2.47 (d, 2H, *J* = 7 Hz), 1.85 (m, 1H), 1.53 (d, 3H, *J* = 7 Hz), 1.35 (d, 3H, *J* = 7 Hz), 0.93 (d, 6H, *J* = 7 Hz). Anal. (C₁₆H₂₃NO₃) C, H, N.

3-[4-((R)-2-(Methylsulfonylamino)-1-methyl-2-oxoethyl)phenyl]-2-methylpropionic Acid (10). Compound **10** was isolated by extraction from the collected urine of three rats treated with compound **2** (1 g/die) for a single day. The collected urine (about 30 mL) was acidified with 37% HCl and extracted with EtOAc (2 × 15 mL). The collected organic extracts were dried over Na₂SO₄, and the solvent was evaporated under vacuum. Pure **10**, as mixture of diastereoisomers, was isolated by silica gel column chromatography (eluting mixture CHCl₃:MeOH, 9:1) as a white solid (0.65 g, 2.07 mmol): mp 127–140 °C (diastereoisomers mixture); ¹H NMR (CDCl₃) δ 8.20 (bs, 1H, CONH), 7.12 (s, 4H), 3.66 (q, 1H, *J* = 7 Hz), 3.21 (s, 3H), 3.01 (m, 1H), 2.78 (m, 2H), 1.51 (d, 3H, *J* = 7 Hz), 1.23 (dd, 3H, *J*₁ = 7 Hz, *J*₂ = 5 Hz). Anal. (C₁₄H₁₉NO₅S) C, H, N.

Diastereoisomeric purity was assayed by HPLC–UV (Chiralcel OJ column, eluting mixture 75:15:10 *n*-hexane:EtOH:PrOH and 0.5% trifluoroacetic acid), and *t*_R values for [2*R*,2'(*R*,*S*)] were 8.4 and 9.4 min, the ratio being 55:45.

Supporting Information Available: Elemental analyses of the described compounds. This material is available free of charge via the Internet at <http://pubs.acs.org>.

References

- Peters, T. *All about Albumin: Biochemistry, Genetics and Medical Applications*; Academic Press: San Diego, CA, 1996.
- Carter, D. C.; Ho, J. X. Structure of serum albumin. *Adv. Protein Chem.* **1994**, *45*, 153–203.
- Watanabe, H.; Tanase, S.; Nakajou, K.; Maruyama, T.; Kragh-Hansen, U.; Otogiri, M. Role of Arg-410 and Tyr-411 in human serum albumin for ligand binding and esterase-like activity. *Biochem. J.* **2000**, *349*, 813–819.
- He, X. M.; Carter, D. C. Atomic structure and chemistry of human serum albumin. *Nature* **1992**, *358*, 209–215.
- Sugio, S.; Mochizuki, S.; Noda, M.; Kashima, A. Crystal structure of human serum albumin at 2.5 Å resolution. *Protein Eng.* **1999**, *12*, 439–446.
- Petitpas, I.; Bhattacharya, A. A.; Twine, S.; East, M.; Curry, S. Crystal structure analysis of warfarin binding to human serum albumin: Anatomy of drug site I. *J. Biol. Chem.* **2001**, *276*, 22804–22809.
- Gerig, J. T.; Katz, R. E.; Reinheimer, J. D.; Sullivan, J. R.; Roberts, J. D. Examination of the aspirin acetylation site of HSA by ¹³C NMR spectroscopy. *Org. Magn. Reson.* **1981**, *15*, 158–161.
- Diaz, N.; Suarez, D.; Sordo, T. L. Theoretical study of the water-assisted aminolysis of β-lactams: Implications for the reaction between human serum albumins and penicillins. *J. Am. Chem. Soc.* **2000**, *122*, 6710–6719.
- Diaz, N.; Suarez, D.; Sordo, T. L.; Merz, K. M. Molecular dynamics study of the binding site in human serum albumin: Influence of the protonation state of Lys195 and Lys199. *J. Med. Chem.* **2001**, *44*, 250–260.
- Bhattacharya, A. A.; Curry, S.; Franks, N. P. Binding of the general anesthetics propofol and halothane to human serum albumin. High-resolution crystal structures. *J. Biol. Chem.* **2000**, *275*, 38731–38738.
- Domenici, E.; Bertucci, C.; Salvadori, P.; Wainer, I. W. Use of a human serum albumin-based chiral stationary phase for high performance liquid chromatography for the investigation of protein binding: Detection of the allosteric interaction between warfarin and benzodiazepine binding sites. *J. Pharm. Sci.* **1991**, *80*, 164–169.
- Colmenarejo, G.; Alvarez-Pedraglio, A.; Lavandera, J. L. Chem-informatic models to predict binding affinities to human serum albumin. *J. Med. Chem.* **2001**, *44*, 4370–4378.
- Deschamps-Labat, L.; Péhourcq, F.; Jagou, M.; Bannwarth, B. Relationship between lipophilicity and binding to human serum albumin of arylpropionic acid nonsteroidal and antiinflammatory drugs. *J. Pharm. Biomed. Anal.* **1997**, *16*, 223–229.
- Kratochwil, N. A.; Huber, W.; Müller, F.; Kansy, M.; Gerber, P. R. Predicting plasma protein binding of drugs: A new approach. *Biochem. Pharmacol.* **2002**, *64*, 1355–1374.
- Ermondi, G.; Lorenti, M.; Caron, G. Contribution of ionization and lipophilicity to drug binding to albumin: A preliminary step toward biodistribution prediction. *J. Med. Chem.* **2004**, *47*, 3949–3961.
- Rahim, S.; Aubry, A. F. Location of binding sites on immobilized human serum albumin for some nonsteroidal antiinflammatory drugs. *J. Pharm. Sci.* **1995**, *84*, 949–952.
- Allegretti, M.; Cesta, M. C.; Bizzarri, C.; Sabbatini, V.; Bertini, R.; Caselli, G.; Gandolfi, C. Amides of *R*-2-(aminoaryl)-propionic acids for use in the prevention of leucocyte activation. WO0179189, 2001.
- Schadendorf, D.; Moller, T.; Algermissen, B.; Worm, M.; Sticherling, M.; Czarnetzki, B. M. IL-8 produced by human malignant melanoma cells in vitro is an essential autocrine growth factor. *J. Immunol.* **1993**, *151*, 2667–2675.
- Lee, J.; Horuk, R.; Rice, G. C.; Bennett, G. L.; Camerato, T.; Wood, W. I. Characterization of two high affinity human interleukin-8 receptors. *J. Biol. Chem.* **1992**, *15*, 16283–16287.
- Bizzarri, C.; Allegretti, M.; Di Bitondo, R.; Cervellera, M. N.; Colotta, F.; Bestini, R. Pharmacological inhibition of Interleukin-8 (CXCL8) as a new approach for the prevention and treatment of several human diseases. *Curr. Med Chem.-Anti-inflammatory Anti-Allergy Agents* **2003**, *2*, 67–79.
- Liu, Z.; Giudice, G. J.; Zhou, X.; Swartz, S. J.; Troy, J. L.; Fairley, J. A.; Till, G. O.; Diaz, L. A. A major role for neutrophils in experimental bullous pemphigoid. *J. Clin Invest.* **1997**, *100*, 1256–1263.
- Bertini, R.; Allegretti, M.; Bizzarri, C.; Moriconi, A.; Locati, M.; Zampella, G.; Cervellera, M.; Di Ciccio, V.; Cesta, M.; Galliera, E.; Martinez, F.; Di Bitondo, R.; Troiani, G.; Sabbatini, V.; D'Annibale, G.; Anacardio, R.; Cutrin, J.; Cavalieri, B.; Mainiero, F.; Stripoli, R.; Villa, P.; Di Girolamo, M.; Martin, F.; Gentile, M.; Santoni, A.; Corda, D.; Poli, G.; Mantovani, A.; Ghezzi, P.; Colotta, F. A new class of non-competitive allosteric inhibitors of the inflammatory chemokine receptors CXCR1 and CXCR2: Prevention of reperfusion injury. *Proc. Natl. Acad. Sci. U.S.A.* **2004**, *101*, 11791–11796.
- Oprea, T. I.; Waller, C. L. Theoretical and Practical aspects of three-dimensional Quantitative Structure–Activity Relationships. In *Reviews in Computational Chemistry*; Lipkowitz, K. B., Boyd D. B., Eds.; Wiley-VCH: New York, 1997; 11, pp 127–182.
- Mao, H.; Hajduk, P. J.; Craig, R.; Bell, R.; Borre, T.; Fesik, S. W. Rational design of diflunisal analogues with reduced affinity for human serum albumin. *J. Am. Chem. Soc.* **2001**, *123*, 10429–10435.
- Benet, L. Z.; Øie, S.; Schwartz, J. B. Design and optimization of dosage regimens; pharmacokinetic data. In *The Pharmacological Basis of Therapeutics*; 9th ed.; Gilman's, A. G., Goodman, L. S., Eds.; McGraw-Hill: New York, 1998; pp 1707–1792.
- SYBYL, Molecular Modelling Software, version. 6.9.2; Tripos Assoc.: St. Louis, Missouri.
- CONFORT, Molecular Modelling Software, version 6.0; Tripos Assoc.: St. Louis, Missouri.
- GRID, version 22; available from Molecular Discovery Ltd.: London, U.K. (www.moldiscovery.com).
- VOLSURF, version 4.0; available from Molecular Discovery Ltd.: London, U.K. (www.moldiscovery.com).
- ALMOND, version 3.2.0; available from Molecular Discovery Ltd.: London, U.K. (www.moldiscovery.com).
- GOLPE, version 4.5; available from Multivariate Infometric Analysis srl: Perugia, Italy. (www.miasrl.com).
- <http://www.rcsb.org/pdb>.
- Goodford, P. J. A computational procedure for determining energetically favorable binding sites on biologically important macromolecules. *J. Med. Chem.* **1985**, *28*, 849–857.
- Wade, R. C.; Clark, K. J.; Goodford, P. J. Further development of hydrogen bond functions for use in determining energetically favorable binding sites on molecules of known structure. I. Ligand probe groups with the ability to form two hydrogen bonds. *J. Med. Chem.* **1993**, *36*, 140–147.

- (35) Cruciani, G.; Crivori, P.; Carrupt, P. A.; Testa, B. Molecular fields in quantitative structure-permeation relationships: The Volsurf approach. *J. Mol. Struct.* **2000**, *503*, 17–30.
- (36) Crivori, P.; Cruciani, G.; Carrupt, P. A.; Testa, B. Predicting blood-brain barrier permeation from three-dimensional molecular structure. *J. Med. Chem.* **2000**, *43*, 2204–2216.
- (37) Zamora, I.; Oprea, T.; Cruciani, G.; Pastor, M.; Ungell, A. L. Surface descriptors for protein–ligand affinity prediction. *J. Med. Chem.* **2003**, *46*, 25–33.
- (38) Pastor, M.; Cruciani, G.; McLay, I.; Pickett, S.; Clementi, S. GRid-INdependent descriptors (GRIND): A novel class of alignment-independent three-dimensional molecular descriptors. *J. Med. Chem.* **2000**, *43*, 3233–3243.
- (39) Baroni, M.; Costantino, G.; Cruciani, G.; Riganelli, D.; Valigi, R.; Clementi, S. Generating Optimal Linear PLS Estimations (GOLPE): An advanced chemometric tool for handling 3D-QSAR problems. *Quant. Struct.-Act. Relat.* **1993**, *12*, 9–20.
- (40) Cruciani, G.; Clementi, S. GOLPE: Philosophy and Applications in 3D-QSAR. In *Advanced Computer-Assisted Techniques in Drug Discovery*; van de Wateerbremd, H., Ed.; VCH: Weinheim, 1994; pp 61–88.
- (41) Cruciani, G.; Clementi, S.; Baroni, M. Variable Selection in PLS Analysis. In *3D QSAR in Drug Design, Theory, Methods and Applications*; Kubinyi, H., Ed.; ESCOM: Leiden, 1993; pp 551–564.
- (42) Eriksson, L.; Johansson, E.; Kettaneh-Wold, N.; Wold, S. PLS. In *Multi and Megavariate Data Analysis using Projection Methods (PCA & PLS)*; Umetrics AB: Umea, 1999; pp 69–112.
- (43) Kastenholz, M. A.; Pastor, M.; Cruciani, G.; Haaksma, E. E.; Fox, T. GRID/CPCA: A new computational tool to design selective ligands. *J. Med. Chem.* **2000**, *43*, 3033–3044.
- (44) Whitlam, J. B.; Brown, K. F. Ultrafiltration in serum protein binding determinations. *J. Pharm. Sci.* **1981**, *70*, 146–50.
- (45) Bowers, W. F.; Fulton, S.; Thompson, J. Ultrafiltration vs equilibrium dialysis for determination of free fraction. *Clin. Pharmacokinet.* **1984**, *9*, 49–60.
- (46) Kwong, T. C. Free drug measurements: Methodology and clinical significance. *Clin. Chim. Acta* **1985**, *151*, 193–216.
- (47) Akgun, H.; Tozkoparan, B.; Ertan, M.; Aksu, F.; Inan, S. Y. Synthesis of some 2-arylpropionic acid amides as prodrugs. *Arzneimittelforschung* **1996**, *46*, 891–894.

JM049227L